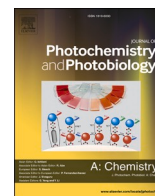




Contents lists available at ScienceDirect

Journal of Photochemistry & Photobiology, A: Chemistry

journal homepage: www.elsevier.com/locate/jphotochem

A Schiff base probe for competitively sensing Cu^{2+} and cysteine through hydrolysis, complexation, and cyclization

Fanyong Yan^{a,*}, Xiaodong Sun^{a,1}, Yan Zhang^a, Yingxia Jiang^a, Li Chen^a, Tengchuang Ma^b, Liang Chen^c

^a State Key Laboratory of Separation Membranes and Membrane Processes/National Center for International Joint Research on Separation Membranes, School of Chemistry and Chemical Engineering, Tiangong University, Tianjin, 300387, PR China

^b Department of Nuclear Medicine, Harbin Medical University Cancer Hospital, Harbin, Heilongjiang, 150081, PR China

^c Graduate School of Life Science, Hokkaido University, Sapporo, 0010024, Japan

ARTICLE INFO

Keywords:

Fluorescent probe
Multistage logical response
Copper ion (II)
Cysteine
Biological imaging

ABSTRACT

The form of a single response to a single target analyte limits the development of fluorescent probes. Here, a probe (HBTA) based on HBT (2-(2-Hydroxyphenyl)-benzothiazole) was synthesized to achieve a concept about nested probe, completing continuous detections. HBTA through low concentration Cu^{2+} gives birth to a new probe (HBT-CHO) that can detect Cu^{2+} by complexation and Cys by cyclization (HBT-Cys). These processes are accompanied by different fluorescent signal changes and can quantitatively detect Cys and Cu^{2+} . Furthermore, HBT-CHO, HBT-Cys, and Cys can bind Cu^{2+} , so competitive fluorescent response of Cu^{2+} can take place through alternate addition of Cu^{2+} and Cys. At this stage, the response becomes too complex to accurately quantify, but it is still dependable to predict changes in the content of the mixture system through competitive fluorescent changes. In summary, it is because of the existence of the nested pattern that HBTA completes multiple forms of responses to Cu^{2+} and Cys.

1. Introduction

Fluorescent probes play vital roles in many areas [1–4], and are attractive to many researchers for their unique sensitivity and selectivity, convenient application, practicality, and economy [5–7]. However, compared to the traditional detection methods, there are drawbacks such as the single-narrow response range due to the limit of their own concentration. Most fluorescent probes have only one response site, which makes them only respond to one analyte and produce enhanced, ratio or quenching fluorescence signals [8–11]. Through designing the structure of fluorescent probes, either by increasing response sites [12–15] or by synergistic interactions with other substances [16], researchers achieved multiple response ranges. In this work, we proposed a nested probe model that can continue to act as a new probe for two or even multiple responses, which provided a way for the problem to some degree.

Many fluorescent probes based on Cu^{2+} have been discovered [17–21]. Complexation were often used to detect Cu^{2+} [22,23], and probes based on the reaction are few. Zhang et al. [24] designed a NIR

probe based on the hydrolysis of ester bonds caused by Cu^{2+} . According to the idea, Gu et al. [7] synthesized a chromene-based probe to detect Cu^{2+} . Zhang et al. [18] designed a reactive probe catalyzed by Cu^{2+} to achieve a bilinear response to Cu^{2+} . Li et al. [25] synthesized a double-responsive probe for detecting Cu^{2+} by using the instability of the imine structure. Additionally, the affinity of imine for Cu^{2+} was discussed in our previous work [26]. In addition, according to literature reports, HBT analogs can complex with Cu^{2+} to form a 2:1 complex [27, 28]. Therefore, the idea that Cu^{2+} can act as a trigger to disintegrate probes to play other roles is feasible. Therefore, HBTA ($\Phi_{\text{HBTA}} = 0.09$) with a double imine structure based on different Cu^{2+} concentrations as triggered signals was designed and synthesized. Detection processes show the corresponding fluorescence signals include enhanced, ratio, and quenching with the continuous increase of the Cu^{2+} concentration. At the same time, the product (HBT-CHO, $\Phi_{\text{HBT-CHO}} = 0.16$) obtained by the reaction of HBTA with 0.1 eq (mole equivalent) of Cu^{2+} carries a formyl group. It is a Cys recognition group and the mechanism has also been proven [29–32]. The respond of HBT-CHO to Cys shows additional ratio-fluorescent changes ($\Phi_{\text{HBT-Cys}} = 0.13$). Moreover, Cys can

* Corresponding author.

E-mail address: yanfanyong@tiangong.edu.cn (F. Yan).

¹ These authors contributed equally to this work.

<https://doi.org/10.1016/j.jphotochem.2020.113065>

Received 10 September 2020; Received in revised form 15 November 2020; Accepted 30 November 2020

Available online 4 December 2020

1010-6030/© 2020 Elsevier B.V. All rights reserved.

competitively complex Cu^{2+} to achieve off-on alternation [33–35], which further adds to functionality and application value of HBTA. Design ideas and the main response methods involved are shown in Scheme 1.

On the other hand, Cu^{2+} as a common cation widely is found in soil [36,37], water [38,39], and organism organisms [40–43]. 20 μM of Cu^{2+} in drinking water was provided by the EPA (US Environmental Protection Agency) [44]. Extra Cu^{2+} in human body affects the nervous system and causes neurological diseases like Parkinson's, Alzheimer's, Menkes' and Wilson's disease [45–48]. As a fundamental thiol-containing amino, Cys acid is concerned with physiological processes such as detoxification, metabolism, protein synthesis and post-translational modification [49,50]. Anomalous Cys levels in human body can cause a variety of diseases including lethargy, edema, slow growth, hair depigmentation, skin lesions, liver damage, Alzheimer's and cardiovascular diseases [51,52]. HBTA realized the continuous detection to Cu^{2+} and Cys and logical fluorescence output according to concentration change and order of addition. Anyway, we hope to provide a new way of designing probes to detect interrelated analytes to play a more important role in environmental, bioimaging, disease treatment, etc.

2. Experiment

2.1. Materials and equipment

Analytical grade 2-aminobenzenethiol was purchased from Aladdin Reagent Co., LTD. Trifluoroacetic Acid (TFA) was purchased from Tianjin Kemiou Chemical Reagent Co., LTD. Hexamethylenetetramine (HMTA) was purchased from Tianjin Guangfu Technology Development Co., LTD. Other solvents and test agents were purchased from Tianjin fengchuan chemical reagent technology Co., LTD. All chemicals were used without further purification. Thin layer chromatography (TLC) and column chromatography (200–300 mesh silica gel) were purchased from Qingdao ocean chemical Co., LTD and was used to monitor reactions and purify the products.

IR spectra were obtained by a TENSOR37 FT-IR through KBr disks. ^1H NMR were measured with a Bruker Advance III HD 400 MHz spectrometer in DMSO- d_6 (TMS as an internal standard). The UV–vis spectra were obtained by Purkinje General TU-1901 UV–vis spectrophotometer. The fluorescence spectra were obtained by F-380 fluorescence spectrophotometer. HRMS was obtained by Bruker micro TOF-QII instrument. Standard quartz cuvettes of 1 cm path length were used in all optical measurement. The pH was carried out on a Mettler Toledo pH meter.

E. coli bioimaging was obtained through an upright fluorescence microscope (Olympus bx 53). All cells were observed by the Leica SP5 confocal microscopy. Reaction intermediates was determined though UPLC-MS data by UPLC H-CLASS Xevo TQ-D MS.

2.2. Quantum yield measurement

Quinine sulfate as a reference ($\Phi = 0.54$), the fluorescence quantum yield (Φ) is calculated according to Eq. (1). Specifically, Quinine sulfate was tested in 0.1 mol L $^{-1}$ H_2SO_4 solution, and probes (HBTA, HBT-CHO, and HBT-Cys) in this experiment was dissolved in Tris/MeOH (v/v = 9/1, 50 mM, pH = 7.4). Five concentration gradients of probes and quinine sulfate were made. The absorbance in the 10 mm cuvette was kept under 0.05 for quinine sulfate and 0.1 for probes to minimize the re-absorption effects. The integrated fluorescence intensity is the integral area of the fluorescence spectrum at the optimal excitation wavelength. Then the graph was plotted using the integrated fluorescence intensity against the absorbance and the intercept is zero.

$$\Phi_x = \Phi_{st} \frac{\text{Grad}_x}{\text{Grad}_{st}} \left(\frac{\eta_x}{\eta_{st}} \right)^2 \quad (1)$$

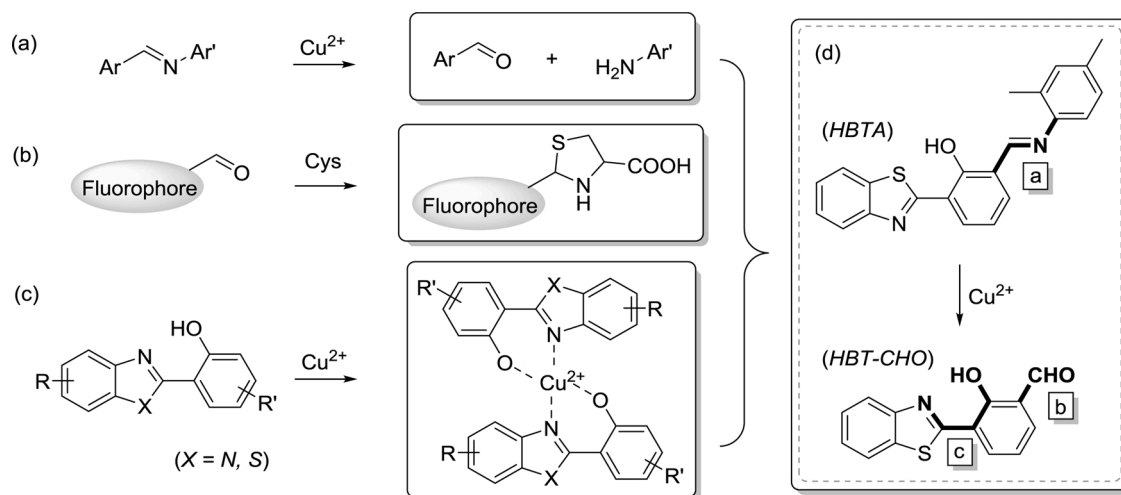
Where Φ is the quantum yield, Grad is the gradient from the plot of integrated fluorescence intensity vs absorbance, η is refractive index of the solvent. The subscript "st" refer to quinine sulfate and "x" refer to the sample.

2.3. The cell imaging

MDA-MB-231 cells were incubated in an *in-vitro* incubator under humidified 5% CO_2 at 37 °C containing 10 % FBS and Penicillin-Streptomycin Solution. First, Nystatin was added to MDA-MB-231 cells in a 35 mm glass-bottomed petri dish for 30 min, then washed 3 times with PBS, and then 10 μL of HBTA (1 mM,) and nystatin were added for another 30 min. The Cells were divided into three groups as blank, 5 μL of Cu^{2+} (1 mM) + 20 μL of NEM (1 mM), 10 μL of Cys (1 mM) for another 60 min. The extra 10 μL of Cys (1 mM) was added to the group of Cu^{2+} + NEM for 60 min. After washing three times with PBS, fluorescence imaging was performed by a fluorescence confocal microscope.

2.4. Synthesize of 2-(benzo[d]thiazol-2-yl) phenol (HBT)

HBT was synthesized according to a reported method [53]. EtOH solution with salicylaldehyde (2.0 mL, 19.2 mmol) and



Scheme 1. The design idea based on response types. a. Cu^{2+} caused hydrolysis of imine; b. Cyclization between fluorophore containing formyl and Cys; c. HBT analogue complexing Cu^{2+} ; d. Structure of HBTA based on the above reaction mechanisms.

2-aminobenzenethiol (2.0 mL, 18.7 mmol) was stirred for 30 min at rt. Then 30 % H₂O₂ (2.3 mL, 74.8 mmol) and 38 % HCl (1.1 mL, 37.3 mmol) was added with stirring for 2 h under N₂. The reaction mixture was poured into ice water and the pale-yellow solid was precipitated out. The suspension was extracted with ethyl acetate (EtOAc) and water. The organic layer was dried under vacuum after treatment with anhydrous sodium sulphate. The crude product was recrystallized in ethanol to afford a almost white to light yellow crystal (3.5 g, 81.2 % yield).

2.5. Synthesis of 3-(benzo[d]thiazol-2-yl)-2-hydroxybenzaldehyde (HBT-CHO)

HBT-CHO was synthesized according to Duff reaction. HBT (1.0 g, 4.4 mmol) was added to 15 mL TFA solution cooled in ice-bath. HTMA (1.0 g, 7.1 mmol) was added to the solution in 30 min then heated up to 80 °C for 9 h. Then 20 mL 4 N HCl was added to the solution refluxing for 30 min. The hot solution was cooled to RT and extracted with dichloromethane (DCM). The organic layer was dried under vacuum after treatment with anhydrous sodium sulphate to afford a yellow solid. The crude product was purified by column chromatography (silica gel, 100–200 mesh, petroleum ether: ethyl acetate = 5:1, v/v) as yellow solid (0.5 g, 46 % yield).

2.6. Synthesis of 2-(benzo[d]thiazol-2-yl)-6-((2,4-dimethylphenyl) imino) methyl phenol (HBTA)

HBT-CHO (0.2 g, 0.8 mmol) and 2,4-dimethyl aniline (174.6 μL, 1.4 mmol) was added to 40 mL methanol solution. One drop of acetic acid was added to the solution. Then the reaction solution was heated to 70 °C. The reaction was monitored by TLC until the material point disappears (10 h). Then the solution was dried under vacuum to afford a red solid. The crude product was purified by column chromatography (silica gel, 100–200 mesh, petroleum ether: ethyl acetate = 100:1, v/v) to afford a red powder (0.15 g, 55 % yield) ¹H NMR (400 MHz, DMSO-d₆) δ 9.19 (s, 1 H), 8.59 (d, J = 7.7 Hz, 1 H), 8.16 (d, J = 7.9 Hz, 1 H), 8.05 (d, J = 8.1 Hz, 1 H), 7.82 (d, J = 7.5 Hz, 1 H), 7.57–7.49 (m, 2 H), 7.43 (t, J = 7.5 Hz, 1 H), 7.18 (d, J = 13.0 Hz, 2 H), 7.10 (t, J = 7.6 Hz,

1 H), 2.44 (s, 3 H), 2.32 (s, 3 H). ¹³C NMR (101 MHz, DMSO-d₆) δ 163.34 (s), 161.93 (s), 161.44 (s), 151.45 (s), 140.47 (s), 137.24 (s), 135.94 (s), 135.53 (s), 132.70 (s), 131.39 (d, J = 19.6 Hz), 127.80 (s), 126.17 (s), 124.63 (s), 122.18 (s), 121.97 (s), 121.40 (s), 119.04 (s), 117.76 (d, J = 5.8 Hz), 20.62 (s), 17.73 (s). HRMS (ESI) m/z: calcd for C₂₂H₁₉N₂OS [M + H]⁺ 359.1213, found: 359.1215 and C₂₂H₁₈N₂OSNa [M + Na]⁺ 381.1032, found: 381.1035. FTIR (KBr) ν_{max}/cm⁻¹ 3344, 2918, 2851, 1615, 1478, 1427, 1296, 1202, 1109, 1036, 756, 617. M. p. = 138–141 °C. (Scheme S1)

3. Results and discussion

3.1. The segment detection of HBTA on Cu²⁺

Titration experiments of Cu²⁺ were carried out at Tris buffer/MeOH (v/v = 9/1, 50 mM, pH = 7.4). With Cu²⁺ concentration from 0.2–160 μM, the spectra change was displayed at Fig. S5. At different concentration ranges of Cu²⁺, HBTA displayed different fluorescence signal change. Fluorescent color changed from orange to green with the addition of a small amount of Cu²⁺. A ratio response of a linear range between I₅₂₅/I₅₉₀ and concentration of 0.2–1.6 μM was acquired (I₅₂₅/I₅₉₀ = 0.234[Cu²⁺] + 0.69; R² = 0.985). A detection limit of 86.9 nM (3σ/k) was obtained in the concentration range (Fig. 1a and d). At the concentration of 6–12 μM, green fluorescence at 525 nm was continuously enhanced to obtain a linear range (I₅₂₅ = 101.61[Cu²⁺] + 60.29; R² = 0.979). The limit of detection in the range was calculated to be 2.6 nM (3σ/k) (Fig. 1b and e). In Cu²⁺ concentration of 40–160 μM, the green fluorescence was quenched and detection limit was calculated as 87.5 nM (3σ/k) (I₅₂₅ = -3.04[Cu²⁺] + 731.4; R² = 0.997) (Fig. 1c and f). The linearity in the transition phase of these ranges was instable, thus the quantitative detection failure (Fig. S5). This phenomenon of fluorescence signal variation at different Cu²⁺ concentration ranges are in line with our expectation, and these processes will interact with each other.

The prominent lone pair electron and the small steric hindrance of the imine structure makes imine have affinity for Cu²⁺ [26]. Therefore, selective experiment was carried out. A stock solution (2.0 mM) of HBTA was prepared in MeOH. Stock solutions (2.0 mM, high

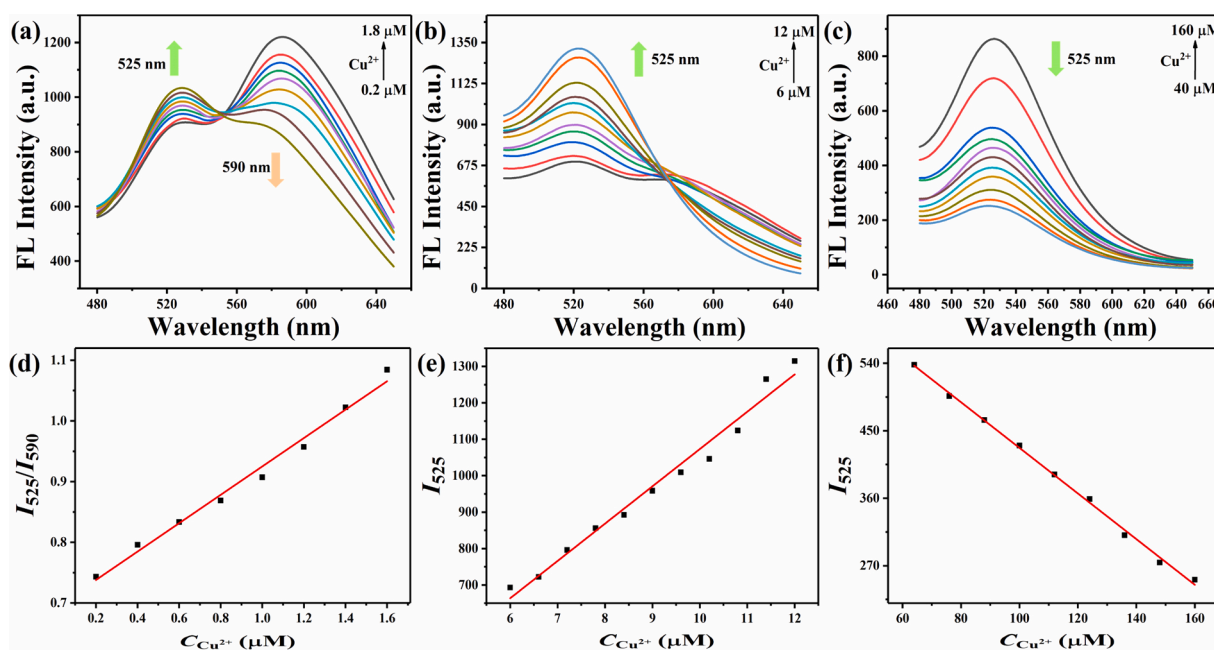


Fig. 1. Fluorescence titration of Cu²⁺ to HBTA (Tris/MeOH v/v = 9/1, 50 mM, pH = 7.4, incubation time: 30 min). a. Fluorescence spectra of HBTA in a Cu²⁺ range of 0.2–1.8 μM (λ_{ex} = 350 nm); b. Fluorescence spectra of HBTA in a Cu²⁺ range of 6–12 μM (λ_{ex} = 400 nm); c. Fluorescence spectra of HBTA in a Cu²⁺ range of 40–160 μM (λ_{ex} = 400 nm); d. Linearity in a Cu²⁺ range of 0.2–1.6 μM; e. Linearity in a Cu²⁺ range of 6–12 μM; f. Linearity in a Cu²⁺ range of 60–160 μM.

concentration) of cation (Na^+ , Mg^{2+} , Al^{3+} , K^+ , Ca^{2+} , Cr^{3+} , Mn^{2+} , Fe^{2+} , Fe^{3+} , Co^{2+} , Ni^{2+} , Cu^{2+} , Zn^{2+} , Ag^+ , Cd^{2+} , Ba^{2+} , Hg^{2+} , and Pb^{2+}) were prepared in distilled water. 200 μL HBTA solution and 200 μL cationic solution were added to a 10 mL volumetric flask with a stock solution of Tris buffer/MeOH ($v/v = 9/1$, 50 mM, $\text{pH} = 7.4$). All ions except Cu^{2+} had no effect on fluorescence of HBTA, and only Cu^{2+} quenched its fluorescence at 590 nm (Fig. 2a). Then competition experiments showed that HBTA had good selectivity to Cu^{2+} (Fig. 2b).

3.2. Effect of Time and pH on detecting Cu^{2+}

The effect of time on probe performance was studied to provide a basis for detection conditions and preliminary mechanism judgment. Three conditions including without Cu^{2+} , 0.1 eq Cu^{2+} , and 2 eq Cu^{2+} were test. In the case of no Cu^{2+} , fluorescence at 525 nm and 590 nm was synchronously reduced for the first 20 min and then remained stable. When 0.1 eq Cu^{2+} was added, fluorescent intensity at 525 nm first increased and then slowly decreased. The fluorescence spectrum remains stable after 30 min. Fluorescent intensity at 590 nm dropped in the first 30 min and then remained stable (Fig. 3b). In Fig. 3c, fluorescence almost disappeared within 50 min and remained stable when 2 eq Cu^{2+} were added. It was as expected that low concentrations of Cu^{2+} can cause decomposition [25] of HBTA and the decomposition product can further complex Cu^{2+} [28].

The effect of pH on the test was carried out as shown in Fig. 3d. Fluorescence intensity at 525 nm and 590 nm were recorded at different pH values. In pH of 7–11, HBTA showed a high degree of quenching and stability for Cu^{2+} . Blank control sample showed a change from orange to green with the change of pH and the fluorescence was green at lower pH (<6.5). The reason for this change in fluorescence under strong acid conditions should be due to the instability of the Schiff base structure on HBTA.

3.3. Detection of Cys after HBTA completes a response to 0.1 eq Cu^{2+}

The formyl group hidden in HBTA was exposed by low concentration of Cu^{2+} . Subsequently, the selective experiment after this response was carried out. Only Cys can cause a new peak at 473 nm among 17 kinds of amino acids (Pro, Trp, Met, Phe, Ala, His, Thr, Arg, Gly, Tyr, Ser, Glu, Asp, GSH, Hcy, Ile, Val), and S^{2-} , SO_3^{2-} (Fig. 4a). Affected by the complicated solution, bad competitive (Fig. S6) and long response time (Fig. 4b) was obtained. The color of the solution no longer changed almost after adding Cys 40 h. A liner relationship between I_{473}/I_{525} and Cys was obtained to be $I_{473}/I_{525} = 0.00363[\text{Cys}] + 0.250$ ($R^2 = 0.987$) in concentration range of Cys in 25–200 μM , and the corresponding

detection limit was calculated to be 5.41 μM ($3\sigma/k$) (Fig. 4c and d). HBT-CHO can cyclize with Cys to form HBT-Cys (MS m/z : HBT-Cys, calcd: 358.04, found: 357.21, Fig. S15) and achieve a fluorescent color from green to blue.

3.4. Mechanism study of HBTA for Cu^{2+} and Cys

To get insight into the reaction mechanism of HBTA with Cu^{2+} and verify the conjecture, nuclear magnetic experiment was carried out as shown in Fig. S7. After adding 0.1 eq of Cu^{2+} , ^1H NMR showed three distinct new peaks: at 10.3 ppm of formyl groups, at 8.3 ppm and 7.8 ppm of benzene ring, and peak at 3.9 ppm of aniline (2,4-dimethyl aniline, MS m/z : $[\text{C}_8\text{H}_{10}\text{N}]^-$ calcd: 120.08, found: 120.49, Fig. S11). Peaks of ^1H NMR belonging to benzene ring were brought together by influence of Cu^{2+} . ^1H NMR results showed that HBTA was disappeared under the action of Cu^{2+} to form its precursor (HBT-CHO, MS m/z : $[\text{C}_{14}\text{H}_8\text{NO}_2\text{S}]^-$ calcd: 254.03, found: 254.03, Fig. S12) with green fluorescence.

In FT-IR spectrum (Fig. S8), hydroxyl peak at 3434 cm^{-1} gradually broadened and formed multiple peaks at 3486 cm^{-1} , 3357 cm^{-1} , and 3167 cm^{-1} eventually as concentration of Cu^{2+} increases. Emerging doublets indicated the formation of primary amines. The movement of hydroxyl peak to high wave number indicated that it participated in complexation of Cu^{2+} . The broadening of these peaks indicated that Cu^{2+} caused an association effect on some groups. The “—C=N—” stretching vibration peak at 1618 cm^{-1} moved to 1641 cm^{-1} , which indicated the involvement in complexation of Cu^{2+} . Peak at 1668 cm^{-1} is a characteristic peak of formyl group indicating disappearance of HBTA in presence of 2 eq Cu^{2+} . The intensity of stretching vibration peak of “C—O” at 1109 cm^{-1} and stretching vibration peak of “C—S” at 617 cm^{-1} were enhanced with increasing Cu^{2+} concentration, which reflected the participation of Cu^{2+} .

From ^1H NMR titration and IR titration spectrum, decomposition of HBTA and formation of HBT-CHO can be inferred. These conclusions can also be obtained by using the changes in UV-vis spectrum (Fig. S9) to give mutual confirmation. Shoulder peak at 282 nm belongs to $\pi-\pi^*$ transition (benzenoid bands) on HBTA benzene ring conjugated system. The peak is inconspicuous due to influence of dimethylaniline. It was blue-shifted after Cu^{2+} indicating that dimethylaniline fall off. The fine structure is to some extent similar with HBT-CHO. Due to formation of formyl group, absorption peak caused by $n-\pi^*$ transition was red shifted from 372 nm to 435 nm according with the UV-vis spectrum of HBT-CHO. Formyl as a chromophore can cause R band to red-shift. The phenomenon is also caused by the generation of the resonance structure belonging to HBTCHO structure with ESIPT process (Fig. S9 Inset). The

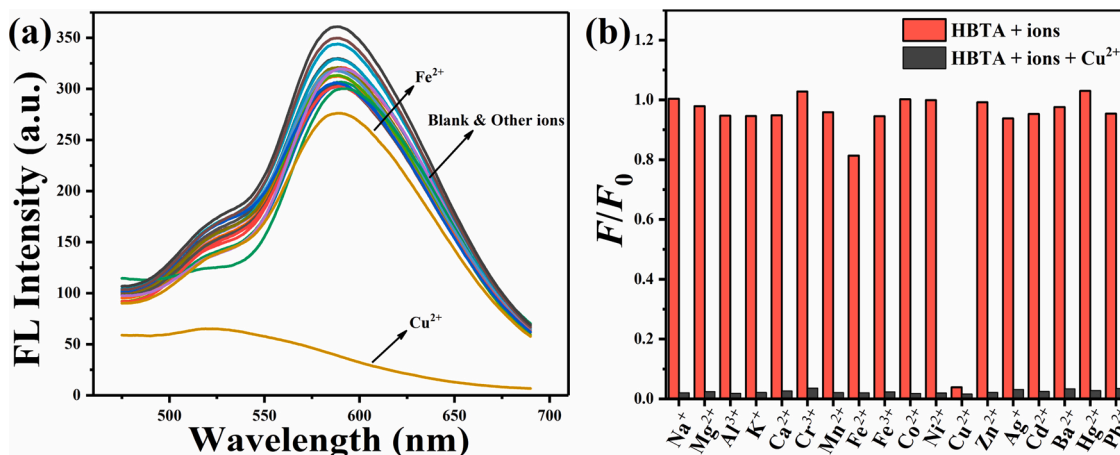


Fig. 2. a. Fluorescence spectra of HBTA (40 μM) upon addition of different cation (40 μM) in Tris buffer/MeOH ($v/v = 9/1$, 50 mM, $\text{pH} = 7.4$, $\lambda_{\text{ex}} = 350\text{ nm}$); b. The F/F_0 value of HBTA + other ions and HBTA + other ions + Cu^{2+} in Tris buffer/MeOH ($v/v = 9/1$, 50 mM, $\text{pH} = 7.4$, $\lambda_{\text{ex}} = 350\text{ nm}$). (incubation time: 30 min).

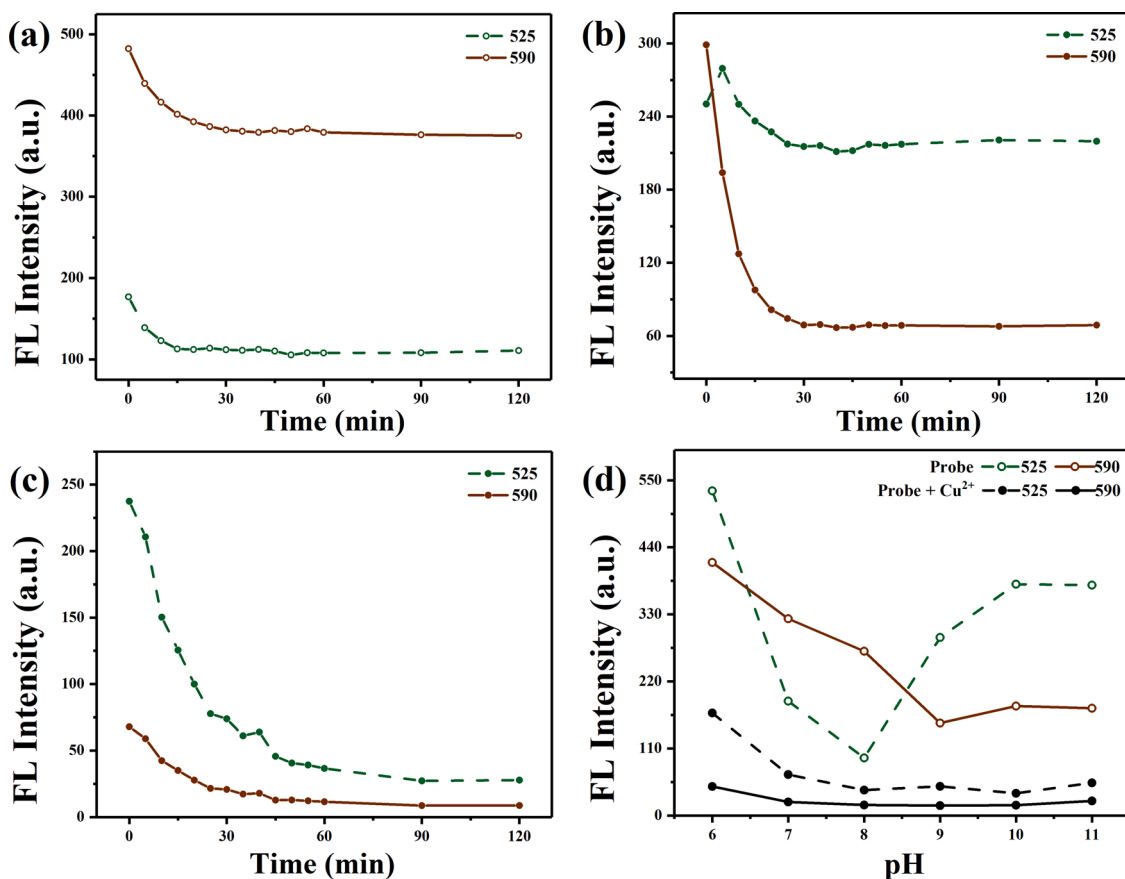


Fig. 3. a. Effect of time on fluorescence of HBTA at 525 nm and 590 nm; b. Effect of time on fluorescence of HBTA at 525 nm and 590 nm after adding 0.1 eq Cu²⁺; c. Effect of time on fluorescence of HBTA at 525 nm and 590 nm after adding 2 eq Cu²⁺; d. Effect of pH (6 – 11) on fluorescence of HBTA at 525 nm and 590 nm after adding 2 eq Cu²⁺ and blank control. (Tris/MeOH v/v = 9/1, 50 mM, pH = 7.4, λ_{ex} = 350 nm).

peak at 435 nm shifted to 400 nm indicating a formation of complex after adding 2 eq Cu²⁺. By comparing UV–vis spectra of HBTA, HBT-CHO and HBTA with Cu²⁺, changes of absorption peak were consistent with previous validation and expectations.

B3LYP/6-31 g(d) was chosen to optimize the ground state structure of the molecule (Fig. S10), and then use the optimized result as the initial value of the excited state to calculate the excited state, and finally get the TD-DFT result. TD-DFT of HBTA and its decomposition product (HBT-CHO) was calculated and shown in Fig. 5. Energy gap was changed from 1.200 eV to 6.595 eV, which indicated that HBT-CHO has a shorter emission wavelength and accords with experimental phenomenon. The narrow band gap of HBTA makes electrons in the ground state more easily excited. Therefore, HBTA molecules exhibit a certain degree of instability. TD-DFT calculation provided a theoretical basis for experimental phenomena and interpretation.

Complexation between HBT-CHO and Cu²⁺ was further studied by Job's and B-H experiments. Detection process of HBTA on Cu²⁺ had been confirmed, then Job's titration was carried out in order to investigate the complex ratio of HBT-CHO to Cu²⁺. A series of solutions, decomposed HBTA and Cu²⁺ with a total concentration of 40 μM were prepared. As proportion of Cu²⁺ concentration increases, the value of $F_0 - F$ reached maximum at abscissa of 0.32 as showed in Fig. 6a. Ratio of HBT-CHO complexing Cu²⁺ was determined to be 2:1 by Job's experiment (2HBT-CHO@Cu²⁺, MS m/z : [C₂₈H₁₇N₂O₄S₂Cu]⁺, calcd: 571.99, found: 572.14, Fig. S13). In B-H experiment, absorption value at 435 nm was continuously decreased and absorption value at 400 nm was increased with the concentration of Cu²⁺, and the isoabsorption point at 410 nm (Fig. 6b). This indicated that HBT-CHO was continuously complexed with Cu²⁺ to form a new complex product. Absorption peak at 400 nm was selected to fit the B-H equation according to previously

reported methods [26] (see ESI). Fitting curve was $y = 184.35x - 47.24$ ($R^2 = 0.987$) (Fig. 6c) and corresponding binding constant was 256.3 M^{-0.5}. Confirmation of complexing process and binding constant is a prerequisite for subsequent competition of Cys for binding to Cu²⁺.

In summary, suggested plausible mechanism of HBTA detection of Cu²⁺ and Cys can be summarized as follows: at low concentrations, Cu²⁺ will first combine with imine of HBTA (HBTA@Cu²⁺, MS m/z : [C₂₂H₁₈NO₂SCu]²⁺, calcd: 421.04, found: 422.40, Fig. S14), and then HBTA initiate decomposition resulting in fluorescence color change [55]. As Cu²⁺ concentration increases, decomposition products begin to complex with Cu²⁺ and dominate whole process, causing fluorescence quenching. On the other way, the decomposition product can detect Cys and generate blue fluorescence (HBT-Cys). The Above process is shown in Scheme 2 and further verified by mass spectrometry. Continuously reaction and complexation of Cu²⁺-responsive probe (HBTA) shows three-stage linear response ranges and three different signal changes [56,57], which indicates its advantages and potentials compared to some Cu²⁺ probes discovered in recent years (Table S1) [58–62].

3.5. HBTA imaging in *E. coli* and MDA-MB-231 cells

In order to preliminarily verify whether HBTA can be applied to organism, *E. coli* imaging experiments were carried out. Slides immobilized with *E. coli* were immersed in HBTA solution for 30 min, and then observed with a fluorescent upright microscope. Rod-shaped *E. coli* was observed in bright and red channels (Fig. S16a and S16b). Slide was removed and placed in a solution containing a low concentration of Cu²⁺ for 30 min. Green and blue fluorescence were observed in the microscope (Figs. S16c and S16d). For comparison, another piece of *E. coli*-loaded slide was immersed in a solution of HBTA treated with

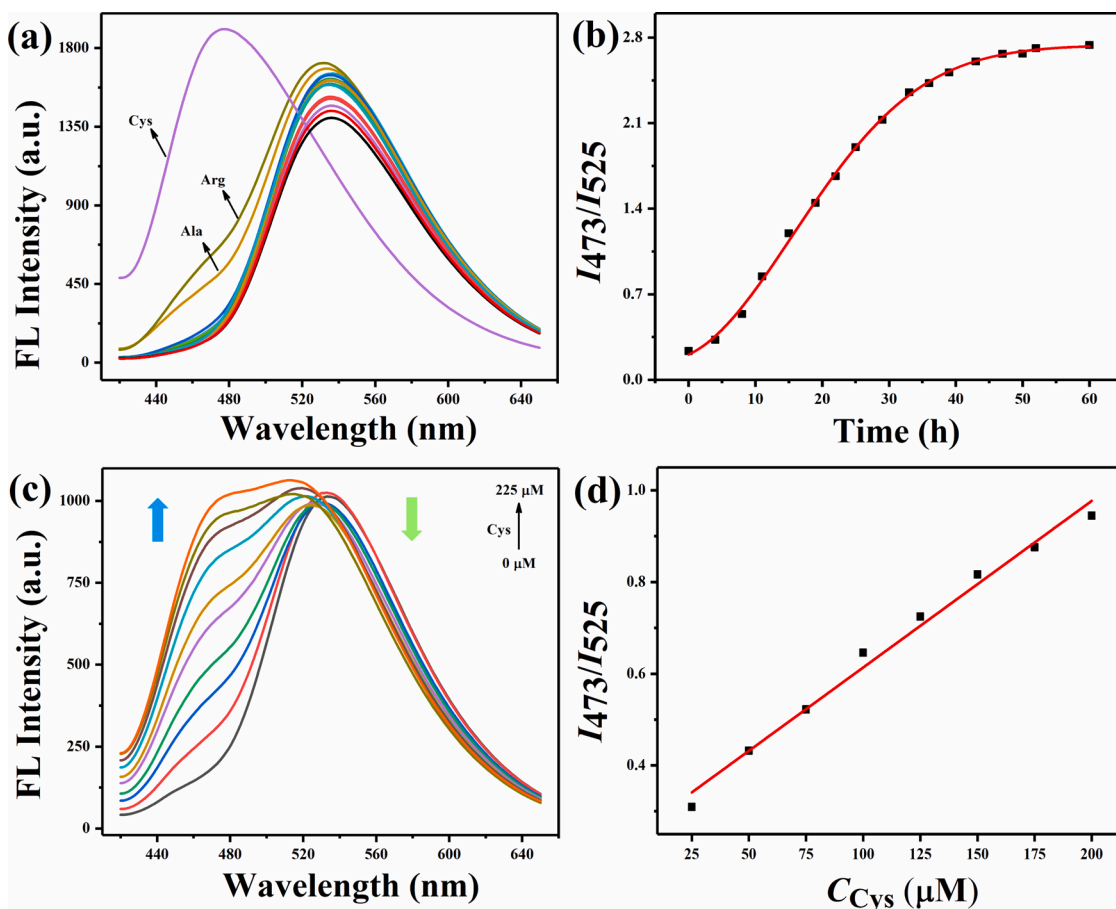


Fig. 4. a. Fluorescence spectra of HBT-CHO (tested after HBT-CHO reacted with 0.1 eq Cu^{2+} in Tris buffer) (10 μM) upon addition of different amino acids (Cys 120 μM) in Tris buffer/MeOH (v/v = 9/1, 50 mM, pH = 7.4, λ_{ex} = 385 nm, after 27 h); b. Value of I_{473}/I_{525} versus time after adding 3 eq Cys; c. Fluorescence changes of HBT-CHO in Cu^{2+} concentration range of 25 – 200 μM (λ_{ex} = 385 nm, after 10 h); d. Linear relationship of Cys in 25 – 200 μM .

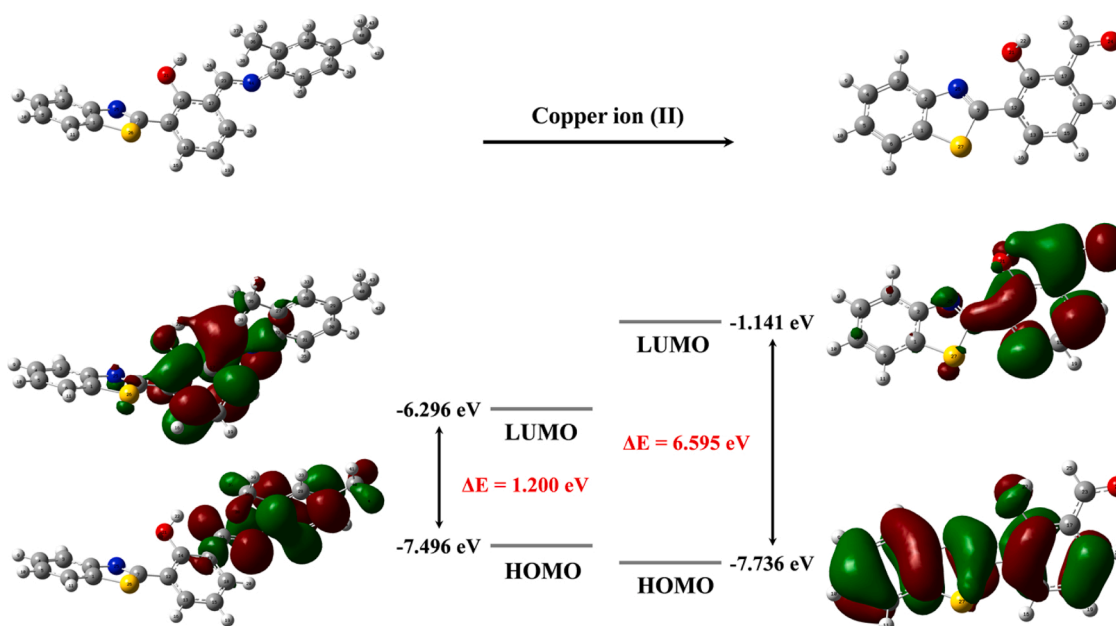


Fig. 5. HOMO-LUMO energy levels and orbitals of HBT-CHO calculated from CAM-B3LYP/6-31G* level of theories.

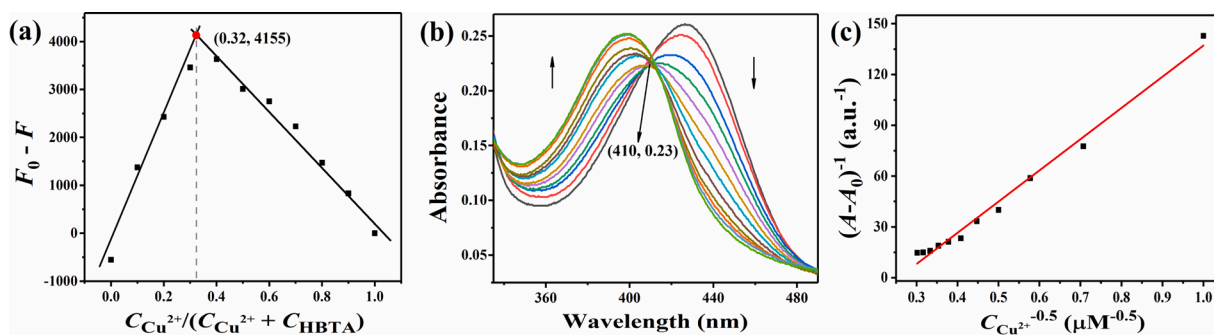
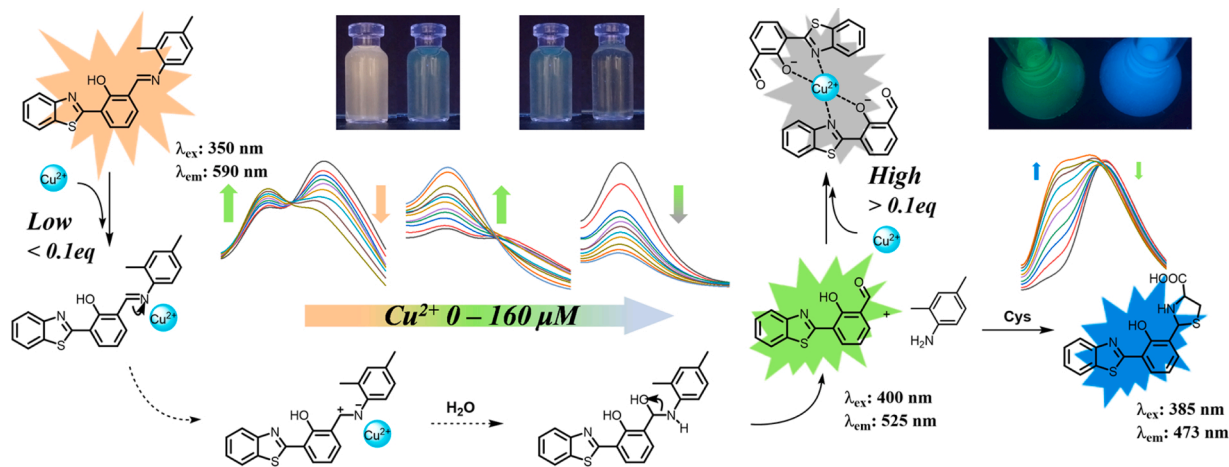


Fig. 6. a. Job's plot of HBT-CHO and Cu^{2+} in solution of Tris/MeOH (v/v = 9/1, 50 mM, pH = 7.4, λ_{ex} = 440 nm); b. UV-vis spectra change from decomposition product of HBTA (20 μM) upon addition of 0 – 11 μM of Cu^{2+} ; c. B-H plot based on a 2:1 association stoichiometry between the decomposition product and Cu^{2+} . (incubation time: 30 min).



Scheme 2. Suggested plausible reaction process of HBTA to Cu^{2+} .

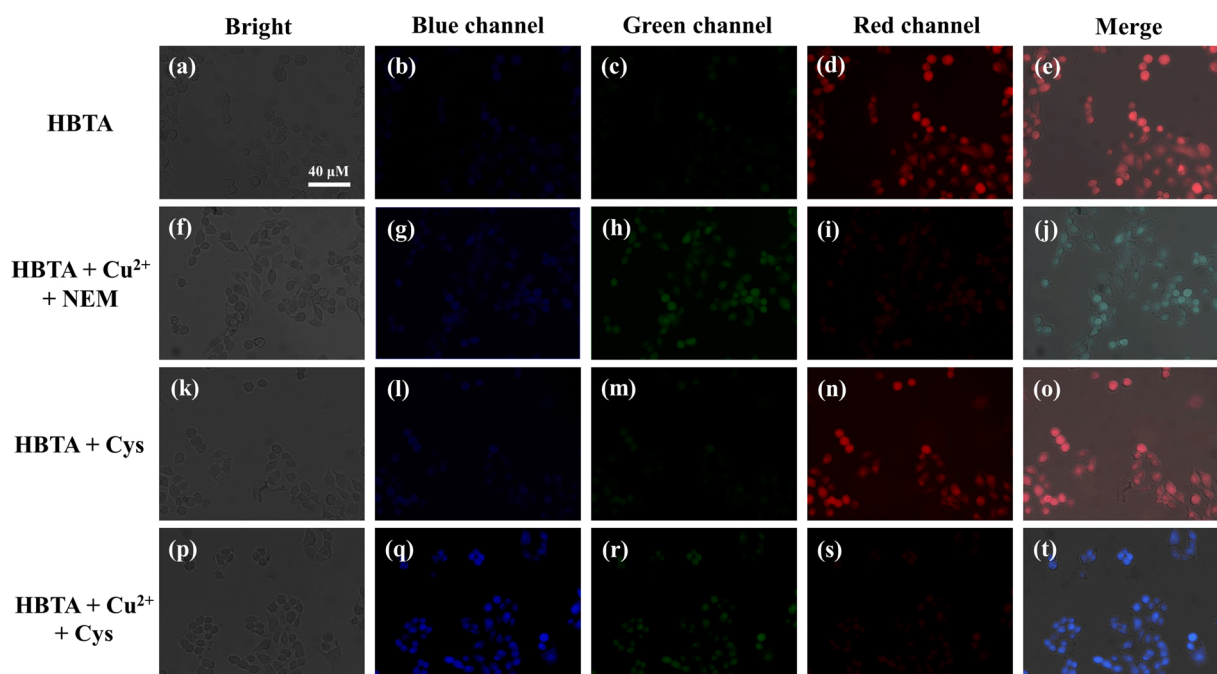


Fig. 7. Confocal fluorescence images at bright, blue channel, green channel, red channel, and merge (left – right, respectively). (a – e). MDA-MB-231 cells incubated with HBTA; (f – j). MDA-MB-231 cells incubated with Cu^{2+} and NEM; (k – o). MDA-MB-231 cells incubated with Cys; (p – t). MDA-MB-231 cells incubated with Cu^{2+} and Cys.

Cu^{2+} . Fluorescent image was observed after 30 min as shown in Fig. S16e and S16f. The results indicated that HBTA can stain *E. coli* and respond to external Cu^{2+} , which revealed that it has potential applications in biological detection.

Then HBTA was used to detect Cu^{2+} and Cys in breast cancer cells (MDA-MB-231). As shown in Fig. S17, cell viability was assessed by MTT assay, and HBTA had low cytotoxicity to the cells. The results of HBTA imaging in cells were shown in the Fig. 7a–e. It can be observed that the cells mainly showed red fluorescence in different channels, which indicated that the cell environment will not cause its decomposition. In order to remove the effect of thiol in cells on the detection of Cu^{2+} by HBTA, NEM together with Cu^{2+} were added to the culture medium. As shown in Fig. 7f–j, the fluorescence in the red channel was weakened, and the green fluorescence was dominant. Therefore, Cu^{2+} -induced decomposition had already taken place. As comparison, the results of culturing Cys with cells without adding Cu^{2+} were shown in Fig. 7k–o. The results were similar to blank experiments, which revealed that only Cys did not cause change color of HBTA in cells. Finally, in order to show that Cys can cause the cyclization process after Cu^{2+} response, Cu^{2+} and Cys were used to culture cells together. As shown in Fig. 7p–t, the blue fluorescence was mainly shown. In summary, HBTA can be used in cells based a nested mode. This logical response made HBTA a potential tool for studying the intrinsic relationship between Cu^{2+} and Cys in organisms [63].

3.6. Competitive fluorescent response

After HBTA was hydrolyzed by Cu^{2+} , HBT-CHO continuedly as a new probe response to Cu^{2+} and Cys achieving different fluorescence signal. Therefore, HBTA can be regard as a secondary probe. Because of the detoxification of Cys to Cu^{2+} *in vivo*, it can adjust the concentration of heavy metal ions. This had been reported in literatures that Cys can complex Cu^{2+} . Based on this, we thought that HBTA could be used as a three-stage even multistage probe. Cu^{2+} and Cys were alternately added to the solution of HBT-CHO. The result showed that green fluorescence was continuously quenched and recovered (Fig. S18a). On the other hand, Cu^{2+} and Cys were alternately added to the solution of HBT-Cys and the blue fluorescence was changed continuously (Fig. S18b).

In above experiments, we had accomplished color change from orange to green to colorless and from orange to green to blue as the signal response. Based on the effect of Cys on Cu^{2+} , we further achieved the color change from orange to green to colorless to green to blue and displayed by fluorescence spectroscopy (Fig. 8a). In addition, changing order of addition achieved the color change from orange to green to blue to colorless to blue (Fig. 8b). The logical relationship diagram be obtained in Fig. 8c and d, which shows the relationship between adding order and amount and fluorescence. Mechanisms and processes are illustrated in Scheme S2 (Scheme 3).

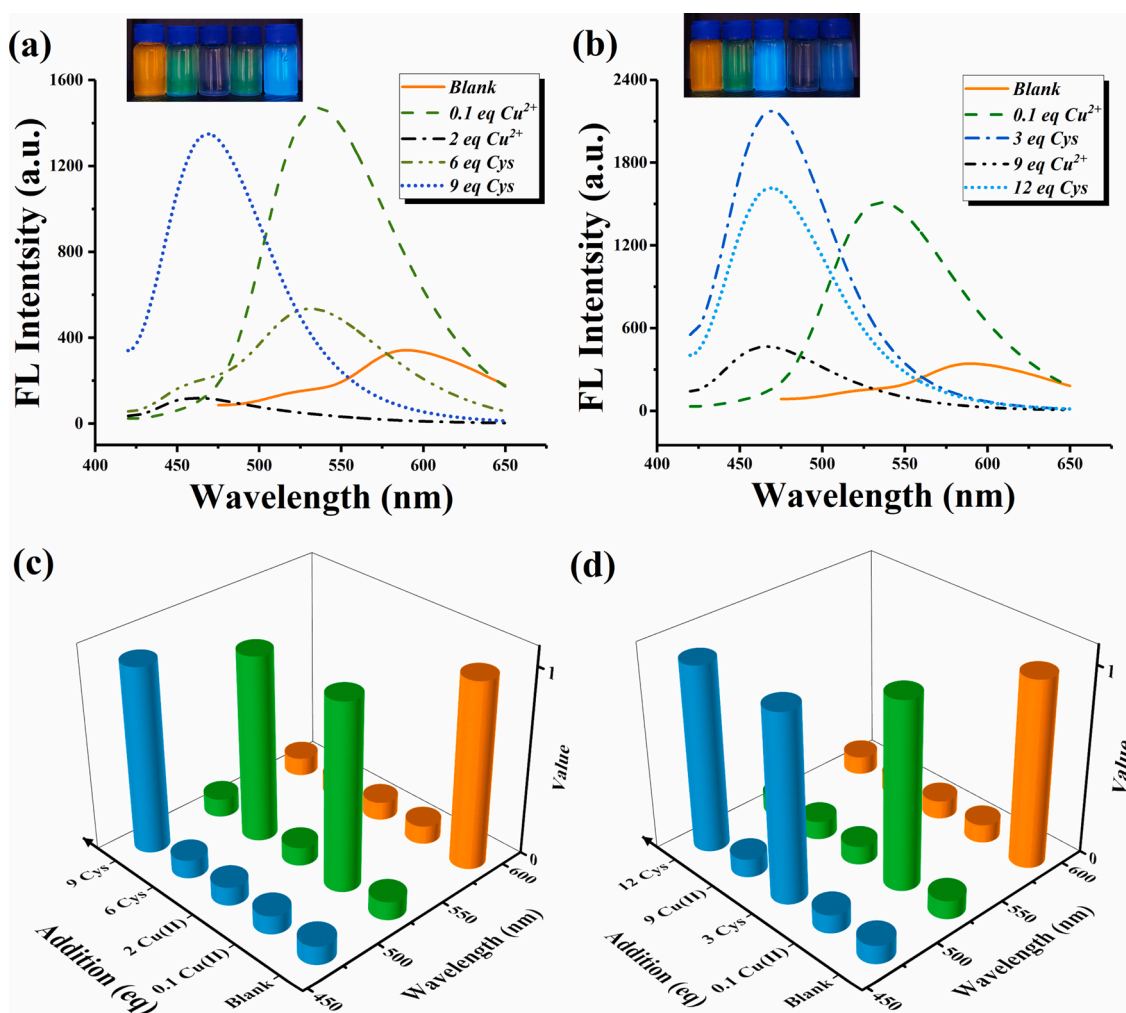
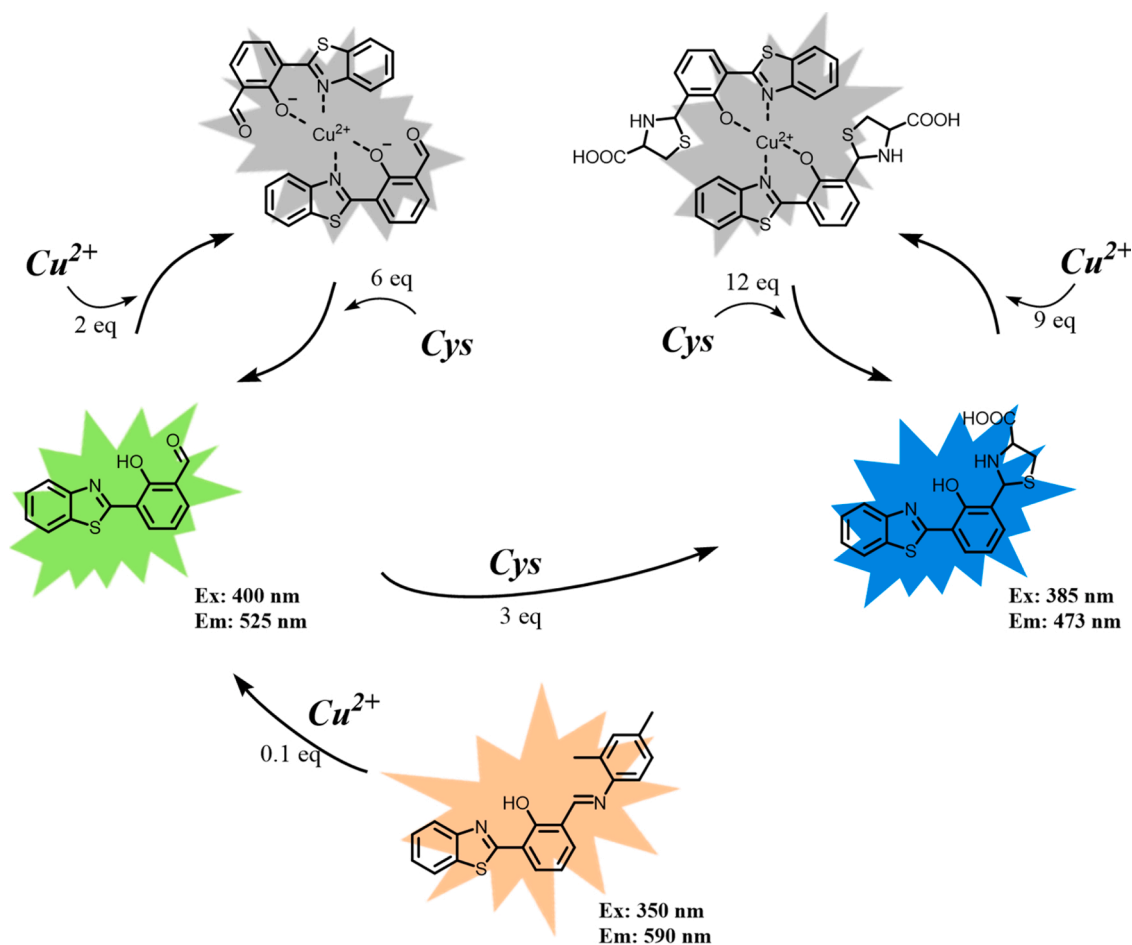


Fig. 8. Fluorescence spectrum changes after adding Cu^{2+} and Cys. a. Changes of fluorescence spectrum based on the addition order of 0.1 eq Cu^{2+} , 2 eq Cu^{2+} , 6 eq Cys and 9 eq Cys (inset: photos of fluorescent change); b. Changes of fluorescence spectrum based on the addition order of 0.1 eq Cu^{2+} , 3 eq Cys, 9 eq Cu^{2+} and 12 eq Cys (inset: photos of fluorescent change); c. Color change according to the addition order of 0.1 eq Cu^{2+} , 2 eq Cu^{2+} , 6 eq Cys and 9 eq Cys; d. Color change according to the addition order of 0.1 eq Cu^{2+} , 3 eq Cys, 9 eq Cu^{2+} and 12 eq Cys.



Scheme 3. Suggested plausible response processes of HBTA with Cu^{2+} and Cys.

4. Conclusion

Inspired by instability and affinity of imine structure to Cu^{2+} , a nested fluorescence probe was designed for breaking the single response defect of current fluorescence probes. According to design ideas, HBTA had achieved a three-stage response to Cu^{2+} including ratio, enhancement, and quenching based on hydrolysis and complexation. The LOD of responses are 86.9 nM, 2.6 nM, and 87.5 nM. The binding ratio of hydrolysate (HBT-CHO) to Cu^{2+} is 2: 1 and the binding constant is $256.3 M^{-0.5}$. In addition, HBT-CHO can selectively detect Cys through cyclization with a formyl group to achieve fluorescent change from green to blue and the LOD is 5.4 μM . Based on the affinity of Cys to Cu^{2+} , HBTA has achieved a logical response of color change corresponds to concentration change of Cu^{2+} and Cys, verifying the feasibility and rich variability of nested probes.

CRedit authorship contribution statement

Fanyong Yan: Conceptualization, Methodology, Software, Software, Validation, Writing - review & editing. **Xiaodong Sun:** Conceptualization, Methodology, Software, Data curation, Writing - original draft, Writing - review & editing. **Yan Zhang:** Data curation, Writing - original draft. **Yingxia Jiang:** Data curation, Writing - original draft. **Li Chen:** Supervision, Software, Validation. **Tengchuang Ma:** Software, Validation, Writing - review & editing, Resources, Visualization. **Liang Chen:** Writing - review & editing.

Declaration of Competing Interest

There are no conflicts to declare.

Acknowledgements

The work was supported by the National Natural Science Foundation of China (51678409, 51638011, 51578375), Tianjin Research Program of Application Foundation and Advanced Technology (19JCYBJC19800, 18JCYBJC87500, 15ZCZDSF00880), State Key Laboratory of Separation Membranes and Membrane Processes (Z1-201507), and the Program for Innovative Research Team in University of Tianjin (TD13-5042).

Appendix A. Supplementary data

Supplementary material related to this article can be found, in the online version, at doi:<https://doi.org/10.1016/j.jphotochem.2020.113065>.

References

- [1] B. Jiang, Y. Yu, X. Guo, Z. Ding, B. Zhou, H. Liang, X. Shen, White-emitting carbon dots with long alkyl-chain structure: effective inhibition of aggregation caused quenching effect for label-free imaging of latent fingerprint, *Carbon* 128 (2018) 12–20.
- [2] H. Feng, Z. Zhang, Q. Meng, H. Jia, Y. Wang, R. Zhang, Rapid response fluorescence probe enabled in vivo diagnosis and assessing treatment response of hypochlorous acid-mediated rheumatoid arthritis, *Adv. Sci.* 5 (2018) 1800397.
- [3] W. Geng, S. Jia, Z. Zheng, Z. Li, D. Ding, D. Guo, A noncovalent fluorescence turn-on strategy for hypoxia imaging, *Angew. Chem. Int. Ed.* 58 (2019) 2377–2381.

- [4] X. Han, R. Wang, X. Song, F. Yu, L. Chen, Evaluation selenocysteine protective effect in carbon disulfide induced hepatitis with a mitochondrial targeting ratiometric near-infrared fluorescent probe, *Anal. Chem.* 90 (2018) 8108–8115.
- [5] L. Chang, Q. Gao, S. Liu, C. Hu, W. Zhou, M. Zheng, Selective and differential detection of Hg^{2+} and Cu^{2+} with use of a single rhodamine hydrazone-type probe in the absence and presence of UV irradiation, *Dye. Pigment.* 153 (2018) 117–124.
- [6] W. Cheng, Y. Xie, Z. Yang, Y. Sun, M. Zhang, Y. Ding, W. Zhang, General strategy for in situ generation of a Coumarin- Cu^{2+} complex for fluorescent water sensing, *Anal. Chem.* 91 (2019) 5817–5823.
- [7] B. Gu, L. Huang, Z. Xu, Z. Tan, H. Meng, Z. Yang, Y. Chen, C. Peng, W. Xiao, D. Yu, H. Li, A reaction-based, colorimetric and near-infrared fluorescent probe for Cu^{2+} and its applications, *Sensor. Actuat. B-Chem.* 273 (2018) 118–125.
- [8] N. Yan, S. Xie, B. Tang, W. Wang, Real-time monitoring of the dissolution kinetics of silver nanoparticles and nanowires in aquatic environments using an aggregation-induced emission fluorogen, *Chem. Commun.* 54 (2018) 4585–4588.
- [9] L. Wu, Y. Wang, T.D. James, N. Jia, C. Huang, A hemicyanine based ratiometric fluorescence probe for mapping lysosomal pH during heat stroke in living cells, *Chem. Commun.* 54 (2018) 518–521.
- [10] F. Yan, Z. Bai, Y. Chen, F. Zu, X. Li, J. Xu, L. Chen, Ratiometric fluorescent detection of copper ions using coumarin-functionalized carbon dots based on FRET, *Sensor. Actuat. B-Chem.* 275 (2018) 86–94.
- [11] F. Yan, Z. Bai, F. Zu, Y. Zhang, X. Sun, T. Ma, L. Chen, Yellow-emissive carbon dots with a large Stokes shift are viable fluorescent probes for detection and cellular imaging of silver ions and glutathione, *Microchim. Acta* 186 (2019) 113.
- [12] P. Wang, Q. Wang, J. Huang, N. Li, Y. Gu, A dual-site fluorescent probe for direct and highly selective detection of cysteine and its application in living cells, *Biosens. Bioelectron.* 92 (2017) 583–588.
- [13] L. He, X. Yang, K. Xu, X. Kong, W. Lin, A multi-signal fluorescent probe for simultaneously distinguishing and sequentially sensing cysteine/homocysteine, glutathione, and hydrogen sulfide in living cells, *Chem. Sci.* 8 (2017) 6257–6265.
- [14] Y. Yue, F. Huo, P. Ning, Y. Zhang, J. Chao, X. Meng, C. Yin, Dual-site fluorescent probe for visualizing the metabolism of cys in living cells, *J. Am. Chem. Soc.* 139 (2017) 3181–3185.
- [15] Y. Yue, F. Huo, F. Cheng, X. Zhu, T. Mafireyi, R.M. Strongin, C. Yin, Functional synthetic probes for selective targeting and multi-analyte detection and imaging, *Chem. Soc. Rev.* 48 (2019) 4155–4177.
- [16] Y. Guo, L. Yang, W. Li, X. Wang, Y. Shang, B. Li, Carbon dots doped with nitrogen and sulfur and loaded with copper(II) as a “turn-on” fluorescent probe for cysteine, glutathione and moccysteine, *Microchim. Acta* 183 (2016) 409–416.
- [17] M. hang, L. Gong, C. Sun, W. Li, Z. Chang, D. Qi, A new fluorescent-colorimetric chemosensor based on a Schiff base for detecting Cr^{3+} , Cu^{2+} , Fe^{3+} and Al^{3+} ions, *Spectrochim. Acta A* 214 (2019) 7–13.
- [18] Z. Zhang, Y. Liu, E. Wang, A highly selective “turn-on” fluorescent probe for detecting Cu^{2+} in two different sensing mechanisms, *Dye. Pigment.* 163 (2019) 533–537.
- [19] S. Erdemir, S. Malkondu, Dual-emissive fluorescent probe based on phenolphthalein appended diaminomaleonitrile for Al^{3+} and the colorimetric recognition of Cu^{2+} , *Dye. Pigment.* 163 (2019) 330–336.
- [20] K.S. Mami, R. Rajamanikandan, B. Murugesapandian, R. Shankar, G. Sivaraman, M. Ilanchelian, S.P. Rajendran, Coumarin based hydrazone as an ICT-based fluorescence chemosensor for the detection of Cu^{2+} ions and the application in HeLa cells, *Spectrochim. Acta A* 214 (2019) 170–176.
- [21] F. Huo, C. Yin, Y. Yang, J. Su, J. Chao, D. Liu, Ultraviolet-Visible Light (UV-Vis)-reversible but fluorescence-irreversible chemosensor for copper in water and its application in living cells, *Anal. Chem.* 84 (2012) 2219–2223.
- [22] J. Li, C. Yin, Cu^{2+} biological imaging probes based on different sensing mechanisms, *Curr. Med. Chem.* 24 (2017) 3958–4002.
- [23] F. Huo, L. Wang, C. Yin, Y. Yang, H. Tong, J. Chao, Y. Zhang, The synthesis, characterization of three isomers of rhodamine derivative and their application in copper (II) ion recognition, *Sensor. Actuat. B-Chem.* 188 (2013) 735–740.
- [24] H. Zhang, L. Feng, Y. Jiang, Y. Wong, Y. He, G. Zheng, J. He, Y. Tan, H. Sun, D. Ho, A reaction-based near-infrared fluorescent sensor for Cu^{2+} detection in aqueous buffer and its application in living cells and tissues imaging, *Biosens. Bioelectron.* 94 (2017) 24–29.
- [25] C. Li, Z. Yang, S. Li, 1,8-Naphthalimide derived dual-functioning fluorescent probe for “turn-off” and ratiometric detection of Cu^{2+} based on two distinct mechanisms in different concentration ranges, *J. Lumin.* 198 (2018) 327–336.
- [26] F. Yan, X. Sun, R. Zhang, Y. Jiang, J. Xu, J. Wei, Enhanced fluorescence probes based on Schiff base for recognizing Cu^{2+} and effect of different substituents on spectra, *Spectrochim. Acta A* 222 (2019) 117222.
- [27] S. Erdemir, B. Tabakci, M. Tabakci, A highly selective fluorescent sensor based on calix[4]arene appended benzothiazole units for Cu^{2+} , S^{2-} and HSO_4^- ions in aqueous solution, *Sensor. Actuat. B-Chem.* 228 (2016) 109–116.
- [28] Y. Li, M. Sun, K. Zhang, Y. Zhang, Y. Yan, K. Lei, L. Wu, H. Yu, S. Wang, A near-infrared fluorescent probe for Cu^{2+} in living cells based on coordination effect, *Sensor. Actuat. B-Chem.* 243 (2017) 36–42.
- [29] Y. Li, A ratiometric fluorescent chemosensor for the detection of cysteine in aqueous solution at neutral pH, *Luminescence* 32 (2017) 1385–1390.
- [30] S. Goswami, A. Manna, S. Paul, A.K. Das, P.K. Nandi, A.K. Maity, P. Saha, A turn on ESIPT probe for rapid and ratiometric fluorogenic detection of homocysteine and cysteine in water with live cell-imaging, *Tetrahedron Lett.* 55 (2014) 490–494.
- [31] C. Yin, K. Xiong, F. Huo, J. Salamanca, R. Strongin, Fluorescent probes with multiple binding sites for the discrimination of Cys, Hcy, and GSH, *Angew. Chem. Int. Ed.* 56 (2017) 13188–13198.
- [32] C. Yin, F. Huo, J. Zhang, R. Martínez, Y. Yang, H. Lv, S. Li, Thiol-addition reactions and their applications in thiol recognition, *Chem. Soc. Rev.* 42 (2013) 6032–6059.
- [33] J. Zong, X. Yang, A. Trinchì, S. Hardin, I. Cole, Y. Zhu, C. Li, T. Muster, G. Wei, Carbon dots as fluorescent probes for “off-on” detection of Cu^{2+} and L-cysteine in aqueous solution, *Biosens. Bioelectron.* 51 (2014) 330–335.
- [34] J. Sun, F. Yang, D. Zhao, C. Chen, X. Yang, Integrated logic gate for fluorescence turn-on detection of histidine and cysteine based on Ag/Au bimetallic nanoclusters- Cu^{2+} ensemble, *ACS Appl. Mater. Inter.* 7 (2015) 6860–6866.
- [35] J. Li, J. Ge, Z. Zhang, J. Qiang, T. Wei, Y. Chen, Z. Li, F. Wang, X. Chen, A cyanine dye-based fluorescent probe as indicator of copper clock reaction for tracing Cu^{2+} -catalyzed oxidation of cysteine, *Sensor. Actuat. B-Chem.* 296 (2019) 126578.
- [36] C.M. Borkert, F.R. Cox, M.R. Tucker, Zinc and copper toxicity in peanut, soybean, rice, and corn in soil mixtures, *Commun. Soil Sci. Plant Anal.* 29 (1998) 2991–3005.
- [37] J. Xu, L. Yang, Z. Wang, G. Dong, J. Huan, Y. Wang, Toxicity of copper on rice growth and accumulation of copper in rice grain in copper contaminated soil, *Chemosphere* 62 (2006) 602–607.
- [38] D. Chen, M. Xu, W. Wu, S. Li, Multi-color fluorescent carbon dots for wavelength-selective and ultrasensitive Cu^{2+} sensing, *J. Alloys. Compd.* 701 (2017) 75–81.
- [39] Y. Shi, Q. Liu, W. Yuan, M. Xue, W. Feng, F. Li, Dye-assembled upconversion nanocomposite for luminescence ratiometric in vivo bioimaging of copper ions, *ACS Appl. Mater. Inter.* 11 (2019) 430–436.
- [40] F. Chen, F. Xiao, W. Zhang, C. Lin, Y. Wu, Highly stable and NIR luminescent Ru-LPMSN hybrid materials for sensitive detection of Cu^{2+} in vivo, *ACS Appl. Mater. Interfaces* 10 (2018) 26964–26971.
- [41] M.L. Desai, B. Deshmukh, N. Lenka, V. Haran, S. Jha, H. Basu, R.K. Singhal, P. K. Sharma, S.K. Kailasa, K. Kim, Influence of doping ion, capping agent and pH on the fluorescence properties of zinc sulfide quantum dots: sensing of Cu^{2+} and Hg^{2+} ions and their biocompatibility with cancer and fungal cells, *Spectrochim. Acta A* 210 (2019) 212–221.
- [42] Z. Guo, Q. Niu, T. Li, E. Wang, Highly chemoselective colorimetric/fluorometric dual-channel sensor with fast response and good reversibility for the selective and sensitive detection of Cu^{2+} , *Tetrahedron* 75 (2019) 3982–3992.
- [43] P. Zhu, Y. Shang, W. Tian, K. Huang, Y. Luo, W. Xu, Ultra-sensitive and absolute quantitative detection of Cu^{2+} based on DNzyme and digital PCR in water and drink samples, *Food Chem.* 221 (2017) 1770–1777.
- [44] T. Lv, Y. Xu, H. Li, F. Liu, S. Sun, A Rhodamine B-based fluorescent probe for imaging Cu^{2+} in maize roots, *Bioorg. Med. Chem.* 26 (2018) 1448–1452.
- [45] Z. Guo, Q. Niu, T. Li, T. Sun, H. Chi, A fast, highly selective and sensitive colorimetric and fluorescent sensor for Cu^{2+} and its application in real water and food samples, *Spectrochim. Acta A* 213 (2019) 97–103.
- [46] H. Jiang, Z. Li, Y. Kang, L. Ding, S. Qiao, S. Jia, W. Luo, W. Liu, A two-photon fluorescent probe for Cu^{2+} based on dansyl moiety and its application in bioimaging, *Sensor. Actuat. B-Chem.* 242 (2017) 112–117.
- [47] A.I. Said, N.I. Georgiev, V.B. Bojinov, The simplest molecular chemosensor for detecting higher pHs, Cu^{2+} and S^{2-} in aqueous environment and executing various logic gates, *J. Photochem. Photobiol. A* 371 (2019) 395–406.
- [48] B. Tripathi, S. Mehta, A. Amar, J. Gaur, Oxidative stress in *Scenedesmus* sp. during short- and long-term exposure to Cu^{2+} and Zn^{2+} , *Chemosphere* 62 (2006) 538–544.
- [49] F. Yan, X. Sun, F. Zu, Z. Bai, Y. Jiang, K. Fan, J. Wang, Fluorescent probes for detecting cysteine, *Methods Appl. Fluoresc.* 6 (2018) 042001.
- [50] M. Jia, L. Niu, Y. Zhang, Q. Yang, C. Tung, Y. Guan, L. Feng, BODIPY-based fluorometric sensor for the simultaneous determination of Cys, Hcy, and GSH in human serum, *ACS Appl. Mater. Inter.* 7 (2015) 5907–5914.
- [51] S. Shahrokhian, Lead phthalocyanine as a selective carrier for preparation of a cysteine-selective electrode, *Anal. Chem.* 73 (2001) 5972–5978.
- [52] M. Liu, N. Li, Y. He, Y. Ge, G. Song, Dually emitting gold-silver nanoclusters as viable ratiometric fluorescent probes for cysteine and arginine, *Microchim. Acta.* 185 (2018) 147.
- [53] S. Sahana, G. Mishra, S. Sivakumar, P.K. Bharadwaj, A 2-(2'-hydroxyphenyl) benzothiazole (HBT)-quinoline conjugate: a highly specific fluorescent probe for Hg^{2+} based on ESIPT and its application in bioimaging, *Dalton Trans.* 44 (2015) 20139–20146.
- [55] D. Udhayakumari, V. Inbaraj, A review on schiff base fluorescent chemosensors for cell imaging applications, *J. Fluoresc.* 30 (2020) 1203–1223.
- [56] D. Udhayakumari, S. Naha, S. Velmathi, Colorimetric and fluorescent chemosensors for Cu^{2+} . A comprehensive review from the years 2013–2015, *Anal. Methods* 9 (2017) 552–578.
- [57] B. Kaur, N. Kaur, S. Kumar, Colorimetric metal ion sensors – a comprehensive review of the years 2011–2016, *Coord. Chem. Rev.* 358 (2018) 13–69.
- [58] Y. Guo, L. Wang, J. Zhuo, B. Xu, X. Li, J. Zhang, Z. Zhang, H. Chi, Y. Dong, G. Lu, A pyrene-based dual chemosensor for colorimetric detection of Cu^{2+} and fluorescent detection of Fe^{3+} , *Tetrahedron Lett.* 58 (2017) 3951–3956.
- [59] S. Sakunkaewkasem, A. Petdum, W. Panchan, J. Sirirak, A. Charoenpanich, T. Sooksimuang, N. Wanichacheva, Dual-analyte fluorescent sensor based on [5] helicene derivative with super large stokes shift for the selective determinations of Cu^{2+} or Zn^{2+} in buffer solutions and its application in a living cell, *ACS Sens.* 3 (2018) 1016–1023.
- [60] N. Wang, Y. Liu, Y. Li, Q. Liu, M. Xie, Fluorescent and colorimetric sensor for Cu^{2+} ion based on formaldehyde modified hyperbranched polyethylenimine capped gold nanoparticles, *Sensor. Actuat. B-Chem.* 255 (2018) 78–86.

- [61] X. Wei, H. Xu, W. Li, Z. Chen, Colorimetric visualization of Cu^{2+} based on Cu^{2+} -catalyzed reaction and the signal amplification induced by K^+ -aptamer- Cu^{2+} complex, *Sensor Actuat. B-Chem.* 241 (2017) 498–503.
- [62] J. Qiu, S. Jiang, B. Lin, H. Guo, F. Yang, An unusual AIE fluorescent sensor for sequentially detecting Co^{2+} - Hg^{2+} - Cu^{2+} based on diphenylacrylonitrile Schiff-base derivative, *Dye. Pigment.* 170 (2019) 107590.
- [63] Y. Zhang, X. Zeng, L. Mu, Y. Chen, J.-X. Zhang, C. Redshaw, G. Wei, Rhodamine-triazine based probes for Cu^{2+} in aqueous media and living cells, *Sensor Actuat. B-Chem.* 204 (2014) 24–30.